Journal of Colloid and Interface Science 394 (2013) 619–629

Contents lists available at SciVerse ScienceDirect

Journal of Colloid and Interface Science

www.elsevier.com/locate/jcis

Modeling and simulation of dielectrophoretic particle–particle interactions and assembly

Mohammad Robiul Hossan [a], Robert Dillon [b], Ajit K. Roy [c], Prashanta Dutta [a,*]

[a] Mechanical and Materials Engineering, Washington State University, Pullman, WA 99164-2920, USA
[b] Department of Mathematics, Washington State University, Pullman, WA 99164-3113, USA
[c] Air Force Research Lab, Wright Patterson Air Force Base, OH 45433-7750, USA

ARTICLE INFO

Article history:
Received 30 August 2012
Accepted 12 December 2012
Available online 28 December 2012

Keywords:
Multiple particle interactions
Immersed boundary method
Immersed interface method
Dielectrophoresis
Particle assembly

ABSTRACT

Electric field induced particle–particle interactions and assembly are of great interest due to their useful applications in micro devices. The behavior of particles becomes more complex if multiple particles interact with each other at the same time. In this paper, we present a numerical study of two dimensional DC dielectrophoresis based particle–particle interactions and assembly for multiple particles using a hybrid immersed interface-immersed boundary method. The immersed interface method is employed to capture the physics of electrostatics in a fluid media with suspended particles. Particle interaction based dielectrophoretic forces are obtained using Maxwell's stress tensor without any boundary or volume integration. This electrostatic force distribution mimics the actual physics of the immersed particles in a fluid media. The corresponding particle response and hydrodynamic interactions are captured through the immersed boundary method by solving the transient Navier–Stokes equations. The interaction and assembly of multiple electrically similar and dissimilar particles are studied for various initial positions and orientations. Numerical results show that in a fluid media, similar particles form a chain parallel to the applied electric field, whereas dissimilar particles form a chain perpendicular to the applied electric field. Irrespective of initial position and orientation, particles first align themselves parallel or perpendicular to the electric field depending on the similarity or dissimilarity of particles. The acceleration and deceleration of particles are also observed and analyzed at different phases of the assembly process. This comprehensive study can be used to explain the multiple particle interaction and assembly phenomena observed in experiments.

1. Introduction

Due to a high degree of selectivity and sensitivity, dielectrophoresis (DEP) has become one of the most promising and popular tools for characterization, manipulation, and actuation of biomaterials and biological entities in micro/nanofluidic devices. In dielectrophoresis, an applied electric field polarizes dielectric particles or materials and hence causes a net force due to unequal electric fields on the accumulated charges. This net force drives the particles toward higher or lower electric field regions depending on the properties of the medium and the particles. Dielectrophoresis works both on charged and neutral particles. Since the inception of microfabrication techniques, a growing number of researchers have been using this phenomenon, and many valuable applications such as cell separation [1], sorting [2], trapping [3] as well as isolation [4], concentration [5], and characterization of biological particles [6] have already been demonstrated. In recent years, dielectrophoretic force has also been used for the assembly of colloidal particles into a structure [7], the formation of tissues using biological cells [8], and fabrication of biosensors using DNA/protein molecules [9] .

Dielectrophoretic assembly has better control and faster response rates compared to the other micro/nano assembly processes such as capillary [10], sedimentation [11], chemical [12], and electro-optical [13]. In dielectrophoresis, two major contributing factors are particle polarization and electric field nonuniformity. Particles in a close proximity alter the electric field and create local nonuniformity in the electric field between particles. Due to this asymmetric electric field, dielectrophoresis based particle–particle interaction forces act on each other. This interaction force can be manipulated to assemble micro/nano particles and biological cells. Chung et al. [14] demonstrated the large scale assembly and integration of carbon nanotubes by dielectrophoresis. Velev and Kaler developed an electrically activated biosensor using dielectrophoretic interaction forces with on-chip electronic

* Corresponding author. Fax: +1 509 335 4662.
E-mail address: prashanta@wsu.edu (P. Dutta).

0021-9797/$ - see front matter © 2012 Elsevier Inc. All rights reserved.
http://dx.doi.org/10.1016/j.jcis.2012.12.039

circuits [9]. Using in vitro dielectrophoretic assembly, Gerard et al. [15] created an artificial microenvironment by multilayered cell aggregation for hematon, a blood producing stem cell. Assembly of live cells and functionalized microparticles were reported by Gupta et al. [16].

Despite many engineering and biomedical applications of dielectrophoretic assembly, the underlying fundamental mechanisms behind this self-assembly process have not yet been fully understood due to the complexity of the transient micro/nanoscale physics. The phenomenon becomes more complex with an increase in the number of interacting particles [17]. Along with experimental investigations, many researchers have used numerical techniques to simulate these complex dynamic phenomena since numerical simulations are fast, efficient, and the relevant parameters can be readily changed in a controlled manner. Kang and Li [18] analyzed particle trajectories by balancing Stokes drag and dielectrophoretic forces using similar particles. However, their approximate solution is valid only if the initial gap between particles is larger than the particle size. Moreover, constant Stokes drag is not appropriate for dielectrophoretic particle–particle interaction. Aubry and co-workers [19,20] quantified the inherent dielectrophoretic force and particle–particle interaction force based on two characteristic length scales – spatial nonuniformity of the electric field and the distance between two particles – using Lagrange multiplier methods. They concluded that the particle–particle interaction force can be nullified by selecting an appropriate liquid media so that the Clausius–Mossotti factor becomes small. However, Aubry and co-workers calculated dielectrophoretic forces using a simplified point dipole method which is not valid when particles are close to each other [20]. Recently Ai and Qian [21] studied dielectrophoretic particle–particle interaction with their relative motion in the suspending media using the commercial finite element package COMSOL by adopting the arbitrary Lagrangian–Eulerian (ALE) method. The ALE approach is computationally expensive as it requires continuous remeshing, and it becomes extremely challenging if one has to consider more particles. House et al. [22] studied the dielectrophoretic particle–particle interactions for ellipsoidal particles using the boundary element method. The boundary element method can only be used in a linear problem such as a dielectrophoretic interaction force using a thin electric double layer (EDL) assumption. All these aforementioned numerical studies considered particle–particle interaction and assembly for similar particles only, but these phenomena are quite different for dissimilar particles [23].

In this study, we present a systematic investigation into the fundamental physics behind particle assembly with multiple similar and dissimilar particles using a hybrid immersed boundary and immersed interface method. The immersed boundary method has been demonstrated to be a stable, efficient, and accurate method for fluid flow with solid–fluid interaction, especially in biological applications with moving inner boundaries [24–26]. On the other hand, the immersed interface method, with a fast algorithm, is particularly well suited for the solution of electric field calculations using the Laplace or Poisson equations with large coefficient jumps across the interface [27]. This hybrid method is simpler, computationally less expensive, and more efficient compared to boundary-fitted methods such as ALE methods. This coupled immersed boundary-immersed interface method is capable of capturing the underlying physics of dielectrophoresis for multiple particles, handling the complex shape and geometry of particles as well as various electrode configurations. Multi-particle interaction forces were calculated based on the Maxwell and hydrodynamic stress tensor, and thus, this study has relaxed many simplified and limiting approximations such as the effective dipole moment and Stokes drag assumptions used in earlier studies.

2. Theory

In this study, we assume that the electric field induced particle interaction and particle assembly are attributed only to DC dielectrophoresis, and we neglect other electrokinetic effects such as electrophoresis and electro-osmosis. Electrophoresis can be neglected if the particles are not charged. On the other hand, the electro-osmotic contribution is very minor due to the ultra small electric double layer [21]. The effect of van der Waals force was not considered here as our numerical algorithm requires a finite separation distance (typically a grid spacing) between particle–particle and particle–wall. For the typical grid spacing considered in this study, the van der Waals force as well as the Brownian force is much smaller than the electrostatic and hydrodynamic force [21]. To reduce the computational complexities, we have only considered two dimensional geometries. However, the mathematical models presented in this study can easily be extended to three dimensional objects.

The physics of dielectrophoretic particle assembly can be explained in terms of the charge distribution at the interface between a particle and its suspending media under an external electric field. Because of the different dielectric properties between particles and surrounding liquid, the charge accumulations are uneven and hence produce an induced electric dipole – a net positive charge on one side and a net negative charge on the other side of the particle. Thus, in the presence of a nonuniform electric field, unequal opposing forces are created at the opposite sides of the particle, and the particle experiences a net force. The nonuniformity in the electric field can be imposed externally by geometric or electrode configurations. Alternatively, it can be induced locally due to the presence of another particle in close proximity. The direction of this net force depends on the polarizability of the surrounding media and suspended particle. When a particle is more polarizable compared to the media, the net force is directed toward the higher electric field region and vice versa [23]. Under this dielectrophoretic force, the particle travels within a suspending media, induces a flow in a stationary media, and alters the adjacent flow field in a moving media. Hence, in dielectrophoresis, there are complex interactions among the electric field, the particle positions and orientations, and the hydrodynamic flow field.

2.1. Governing equations and boundary conditions

To develop a mathematical model, we consider two particles suspended in a rectangular domain (Fig. 1a) filled with an incompressible and Newtonian viscous fluid. The particle domains are represented by Ω_p with the particle surfaces represented by Γ_p, $p = 1, \ldots, N_p$, where N_p is the number of suspended particles. Considering the typical applied electric field frequency and the characteristic time scale in microfluidic devices, dielectrophoresis can be described as a combination of a quasi-electrostatic and a flow problem. The governing equation for electric potential distribution for a quasi-electrostatic problem can be described by the Gauss' electrostatic law:

$$\nabla \cdot (\tilde{\varepsilon} \nabla \tilde{\varphi}) = 0. \tag{1}$$

The complex permittivity $\tilde{\varepsilon}$ and the complex potential $\tilde{\varphi}$ are given as

$$\tilde{\varepsilon} = \varepsilon - j\sigma/\omega \tag{2}$$

$$\tilde{\varphi} = \varphi(\vec{x}) e^{j\omega t} \tag{3}$$

where ε is permittivity, σ is electrical conductivity, and t is time. The angular frequency ω is related to frequency f as $\omega = 2\pi f$. In a low frequency range, the electrical conductivity of the system

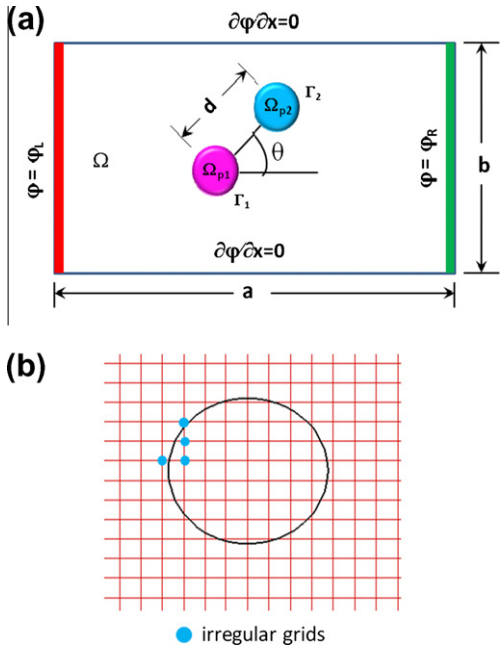

Fig. 1. (a) Schematic of a typical rectangular ($a \times b$) computational domain Ω filled with a liquid to study dielectrophoretic particle assembly of two embedded circular shaped micro particles, Ω_p, (where $p = 1, 2$). Particle boundaries are denoted with Γ. Particles are initially separated by a linear distance d. The initial angle between the line connecting the centerlines of the particles and the applied electric field line is θ. Top and bottom walls are insulated while the left and right boundaries are prescribed with an applied potential. Dirichlet boundary conditions at the right and left boundaries are justified as the electric field is applied through discrete electrodes [23,28]. (b) Schematic of regular and irregular grid points in the immersed interface method. If an interface passes between two grid points then both grid points are irregular.

plays a dominant role in dielectrophoresis, while in high frequency, the permittivity dominates. In case of DC dielectrophoresis, that is, when the frequency becomes zero, the governing equation reduces to

$$\nabla \cdot (\sigma \nabla \varphi) = 0 \tag{4}$$

Since particles are suspended in the fluid media, solution of Eq. (4) requires both boundary and interface conditions. For the system shown in Fig. 1, the boundary conditions are:

$$\varphi(x,y) = \varphi_L \quad \text{at } x = 0 \tag{5a}$$

$$\varphi(x,y) = \varphi_R \quad \text{at } x = a \tag{5b}$$

$$\frac{\partial \varphi(x,y)}{\partial x} = 0 \quad \text{at } y = 0 \text{ and } y = b \tag{5c}$$

The continuity of the electric potential and the normal component of the electric flux density are imposed at every particle material boundary as interface conditions:

$$\varphi_p(x,y) = \varphi_f(x,y) \tag{6a}$$

$$\sigma_p \frac{\partial \varphi_p(x,y)}{\partial \vec{n}} = \sigma_f \frac{\partial \varphi_f(x,y)}{\partial \vec{n}} \tag{6b}$$

where subscripts p is for the particle, f is for the fluid media, and $\vec{n}$ is the surface normal. The electric field $\vec{E}$ is assumed to be irrotational and is calculated as

$$\vec{E} = -\nabla \varphi \tag{7}$$

The dielectrophoretic force can be calculated from Maxwell's stress tensor $\vec{M}$, which is related to the electric field as

$$\vec{F}_{DEP} = \nabla \cdot \vec{M} = \nabla \cdot \left[\varepsilon \vec{E}\vec{E} - \frac{1}{2}(\varepsilon \vec{E} \cdot \vec{E})\vec{I} \right] \tag{8}$$

where $\vec{I}$ is the unit tensor, and $\vec{E}\vec{E}$ is the dyadic product of the electric field. The force $\vec{F}_{DEP}$ obtained from the Maxwell stress tensor includes the force due to inherent nonuniformity in the applied electric field as well as local nonuniformity of the electric field due to the presence of particles or channel walls. The viscous fluid flow is governed by the incompressible Navier–Stokes equations and continuity equation [29]:

$$\rho[\vec{u}_t + (\vec{u} \cdot \nabla)\vec{u}] = -\nabla p + \mu \Delta \vec{u} + \vec{F}(\vec{x}, t) \tag{9}$$

$$\nabla \cdot \vec{u} = 0 \tag{10}$$

where ρ is the fluid density, $\vec{u}$ is the fluid velocity, p is the pressure, and $\vec{F}$ is the body force acting on the fluid. The boundary conditions for the Navier–Stokes equation are given by

$$\left.\begin{aligned} \vec{u} \cdot \vec{n} &= 0 \\ \vec{u} \cdot \vec{\tau} &= 0 \end{aligned}\right\} \quad \text{at } y = 0 \text{ and } y = b \tag{11a}$$

$$\left.\begin{aligned} \vec{u}\ (x = 0, y) &= \vec{u}(x = a, y) \\ \left.\frac{\partial \vec{u}}{\partial y}\right|_{x=0} &= \left.\frac{\partial \vec{u}}{\partial y}\right|_{x=a} \end{aligned}\right\} \quad \text{at } x = 0 \text{ and } x = a \tag{11b}$$

where $\vec{\tau}$ is the unit tangent of the domain boundary. The Eq. (11a) implies no slip and no penetration on the upper and lower domain boundaries, while Eq. (11b) implies periodic boundary conditions on the left and right boundaries of the domain.

3. Numerical method

In this study, two different interface-resolved non-body-fitted grid methods, the immersed boundary method and the immersed interface method, are coupled to study dielectrophoretic particle–particle interaction and assembly. This hybrid method maximizes computational efficiency and reduces computational cost. The electric potential and field distribution are obtained by solving Eq. (4) using the immersed interface method with a fast algorithm. The immersed interface method can handle sharp, rigid or flexible interfaces with large jumps in the coefficients across the interface [27]. The immersed boundary method, used to solve the viscous fluid flow, is simple, easy to implement, and computationally efficient. This method uses a uniform Cartesian grid throughout the computation domain. Before studying the dielectrophoretic assembly, a rigorous grid refinement analysis was performed. Based on the grid refinement analysis, the accuracy of immersed interface method used for the electric potential was found to be second order, and the overall accuracy of the hybrid method was found to be first order due to first order immersed boundary method. This hybrid method has been validated with the experimental results reported in [28] by comparing the experimental levitation of 6 μm latex bead as a function of applied potential on an interdigitized electrode bed. The details of the implementation, convergence analysis, and code validation are presented elsewhere [30]. In this study, the size of the time step was 1e−6 s, while the spatial grid size was 2.9e−7 m.

3.1. Electric field calculation using immersed interface method

The electrostatic problem (Eqs. (4)-(6)) is transformed to an equivalent problem with piecewise constant conductivity and flux interface condition as follows

$$\nabla^2 \varphi = 0 \text{ where } x \in \Omega \tag{12}$$

$$\frac{\partial \varphi_p}{\partial \vec{n}} - \frac{\partial \varphi_f}{\partial \vec{n}} = g(s) \tag{13}$$

where $g(s)$ is the interface jump of the normal derivative of the potential due to the variation of conductivity between the interior and the exterior of the particle. The immersed interface is expressed as a cubic spline passing through a number of control points (X_k, Y_k) for each interface, where $k = 1, 2, \ldots, N$. The discrete form of $g(s)$ can be written as $G = [G_1, G_2, \ldots, G_N]^T$. We employ a uniform Cartesian grid with equal mesh size of h on the domain Ω and using the immersed interface method, and the finite difference formulation of Eq. (12) is given as

$$\frac{\varphi_{i+i,j} + \varphi_{i-1,j} - 4\varphi_{i,j} + \varphi_{i,j+1} + \varphi_{i,j-1}}{h^2} = C_{i,j}, \qquad 1 \leqslant i \leqslant l-1,\ 1 \leqslant j \leqslant n-1 \tag{14}$$

The correction term $C_{i,j}$ is zero except at irregular grid points as shown in Fig. 1b. In matrix–vector form, the finite difference scheme can be written as

$$A\varphi + BG = \lambda \tag{15}$$

where A and B are two matrices, and G is the discrete form of the interface jump condition $g(s)$. BG is the corresponding correction term due to the interface jump condition in Eq. (13). If G is zero, then $A\varphi = \lambda$ is a discrete linear system of finite difference equations without interface. G is determined such that it satisfies the flux continuity in the interface. The interface condition in Eq. (13) can be written in matrix vector form as

$$U\varphi + QG = \gamma \tag{16}$$

where U and Q are matrices, and γ is a vector. These two linear systems of equations are solved simultaneously in two steps. First ϕ is eliminated to obtain a smaller system for G using matrix manipulation as

$$KG = P \tag{17}$$

where $K = (Q - UA^{-1}B)$ and $P = \gamma - UA^{-1}\lambda$. The solution G is obtained using a GMRES routine, where the right hand side and matrix vector multiplication are determined from a weighted least squares interpolation scheme. With the knowledge of G, the solution of the system in Eq. (15) is obtained iteratively through successive calls to the PARDISO solver [31,32]. The details of the immersed interface method with fast algorithm can be found in [27]. With the knowledge of potential distribution from the immersed interface method, the electric field distribution can be obtained using Eq. (7), which will be used to find the dielectrophoretic force.

3.2. Fluid Flow using Immersed boundary method

In the immersed boundary method, the contributions of particles are represented in the fluid domain by a force field, $\vec{F}_{IB}$. The presence of rigid and/or flexible boundaries $\Gamma_p(t)$ of the suspended particles is represented as a singular force

$$\vec{F}_{IB}(\vec{x}, t) = \int_{\Gamma} \vec{f}_{elastic}(s,t)\delta[\vec{x} - \vec{X}(s,t)]ds. \tag{18}$$

Here, $\vec{X}(s,t)$ is a parameterization of $\Gamma_p(t)$, s is a Lagrangian parameter, $\vec{x} = (x, y)$ is spatial position in Eulerian variables, and $\delta(\vec{x})$ is the two dimensional Dirac delta function used to establish communication between Lagrangian and Eulerian variables. The Lagrangian force $\vec{f}(s,t)$ is due to the existence of rigid and flexible immersed boundaries.

The force field $\vec{f}_{elastic}(s,t)$ can be derived from stretching, bending or tethering of immersed boundaries depending on the desired material properties. Hydrodynamic stretching of immersed boundaries generates elastic forces due to the elastic deformation of the particle body. In this study, each immersed point on a boundary is considered to be connected with all other immersed points on that particular particle boundary through elastic links. The elastic force contribution $\vec{f}^{qd}_{elastic}$ of an immersed boundary point $\vec{X}_q$ due to elastic links with the immersed boundary point $\vec{X}_d$ is obtained using Hook's law as follows:

$$\vec{f}^{qd}_{elastic} = S\left(\|\vec{X}_q - \vec{X}_d\| - s_0^{qd}\right)\frac{\vec{X}_q - \vec{X}_d}{\|\vec{X}_q - \vec{X}_d\|} \tag{19}$$

where s_0^{qd} is the resting length between immersed boundary points X_q and X_d. The elastic force at $\vec{X}_d$ due to the elastic link to $\vec{X}_q$ is given by $\vec{f}^{dq}_{elastic} = -\vec{f}^{qd}_{elastic}$. The total elastic force contribution for the immersed boundary point $\vec{X}_q$ is given by $\vec{f}^{q}_{elastic} = \sum_{r=1}^{n_b}\vec{f}^{qd}_{elastic}$, where $d = 1, 2, \ldots, N_p$ and $d \neq q$. In this study, a tether force is employed on the two immersed boundary walls to impose no slip and no penetration boundary conditions in the Navier–Stokes equation. A tether force is applied to each wall immersed boundary point $\vec{X}_q$ with respect to a stationary tether point $\hat{\vec{X}}_q$ using an equation similar to (19), where the resting length s_0^{qd} is set to zero. The Lagrangian elastic and tether forces are interpolated to the Eulerian grid using Eq. (18). The Dirac delta function can be represented as the product of two smooth functions, $\delta_h(\vec{r}) = \delta(x)\,\delta(y)$. The Dirac delta function $\delta_h(\xi)$ with mesh width of h is given by [24]

$$\delta_h(\xi) = \begin{cases} \frac{1}{4h}\left(1 + \cos\left(\frac{\pi\xi}{2h}\right)\right) & \text{if } \|\xi\| < 2h, \\ 0 & \text{if } \|\xi\| \geqslant 2h. \end{cases} \tag{20}$$

This smoothing profile uses only a small number of grid points near the immersed boundary points. Unlike the elastic and tether forces, the dielectrophoretic force density $\vec{F}_{DEP}$ can be obtained directly in Eulerian form from the electric field distribution as [30]:

$$\vec{F}_{DEP} = \nabla\cdot\left[\varepsilon\vec{E}\vec{E} - \frac{1}{2}(\varepsilon\vec{E}\cdot\vec{E})\right] = \varepsilon\frac{\partial\varphi}{\partial x_j}\left(\frac{\partial^2\varphi}{\partial x_i\partial x_i}\right). \tag{21}$$

The total force field due to the presence of immersed boundaries and dielectrophoresis is given by

$$\vec{F} = \vec{F}_{IB} + \vec{F}_{DEP} \tag{22}$$

The governing Eqs. (9) and (10) can be discretized for dielectrophoretic transport of rigid or flexible micro particles with the appropriate force functions described above using finite difference scheme [24–26]. The finite difference discrete form of Eqs. (9) and (10) with a regular mesh width of h is given by

$$\rho\left(\frac{\vec{u}^{\eta+1} - \vec{u}^{\eta}}{\Delta t} + \sum_{\chi=x,y}\vec{u}^{\eta}_{\chi}D^{\pm}_{\chi}\vec{u}^{\eta}\right) = -D^0p^{\eta+1} + \mu\sum_{\chi=x,y}D^{+}_{\chi}D^{-}_{\chi}\vec{u}^{\eta+1} + F^{\eta} \tag{23}$$

$$D^0\vec{u}^{\eta+1} = 0 \tag{24}$$

where χ is the coordinate direction $\chi = x,\ y$, D^+ is the forward difference operator, D^- is the backward difference operator, D^0 is the central difference operator, and $D^{\pm}$ is the upwind difference operator. The transient Navier–Stokes equations are solved using Fast-Fourier-Transform (FFT) methods [25,26,33]. Finally, using the Dirac delta function as described in Equation 18, the velocity of the particle is obtained by advecting the immersed boundary at the local fluid velocity

$$\frac{\partial}{\partial t}\vec{X}(s,t) = \vec{u}[\vec{X}(s,t),t] = \int_{\Omega}\vec{u}(\vec{x},t)\delta[\vec{x} - \vec{X}(s,t)]d\vec{x}, \tag{25}$$

where as in Eq. (18), we use a numerical integration using the discrete representation of $\vec{u}$ and the approximate interpolation function shown in Eq. (20). In IB method, we do not have to deal

with the rotation of particle explicitly since the particle rotation is automatically built into the model as the particles move with the local fluid velocity.

4. Results and discussion

Under an applied electric field randomly orientated particles in a close proximity experience dielectrophoretic particle–particle interaction forces. In this section, we present a numerical analysis of multiple particle–particle interaction using a constant potential difference. We considered a square domain ($a = b = 75$ μm) filled with water; micro particles (12 μm diameter) are immersed within the fluid with several orientations (varying θ) as shown in Fig. 1. The conductivity of the particles was varied from case to case, while the water conductivity ($\sigma_f = 1.0 \times 10^{-4}$ S/m) was fixed. A potential of $\varphi_1 = 1$ V was prescribed at the left electrode, while the right electrode was grounded. The top and bottom boundaries were insulated.

4.1. Similar particle–particle interaction

In the similar particle–particle interaction case, we considered a pair of circular shaped particles with identical electrical properties and dimensions ($d_1 = d_2 = 12$ μm), which are suspended in water. Two different cases were studied for this configuration. In the first case, particles ($\sigma_1 = \sigma_2 = 1.0 \times 10^{-3}$ S/m) were more conductive than the surrounding fluid, while in the second case, particles ($\sigma_1 = \sigma_2 = 1.0 \times 10^{-7}$ S/m) were less conductive than the surrounding fluid. The conductivity of particles considered in the second case corresponds to typical biological cell membrane conductivity.

As particle–particle interactions are mainly driven by the electric field, we begin our analysis with the electric field distribution and the corresponding electrostatic interaction (mutual dielectrophoretic) force between them. Fig. 2a shows the electric field distributions when particles are more conductive than the surrounding media. Due to the higher conductivity of the particles, electric field lines meet the particle surface at right angles. In this case, the tangential component of the electric field is near zero, and particles behave like conductors. Higher electric field regions are created on the left and right sides of the particles. On the other hand, lower electric field regions are created on the top and bottom of the particles. For the second case, where the particle is less conductive than the fluid media, the electric field lines are deflected away from the particle surface (Fig. 2b), and the particles behave like insulators. Thus, the electric field outside the particle becomes

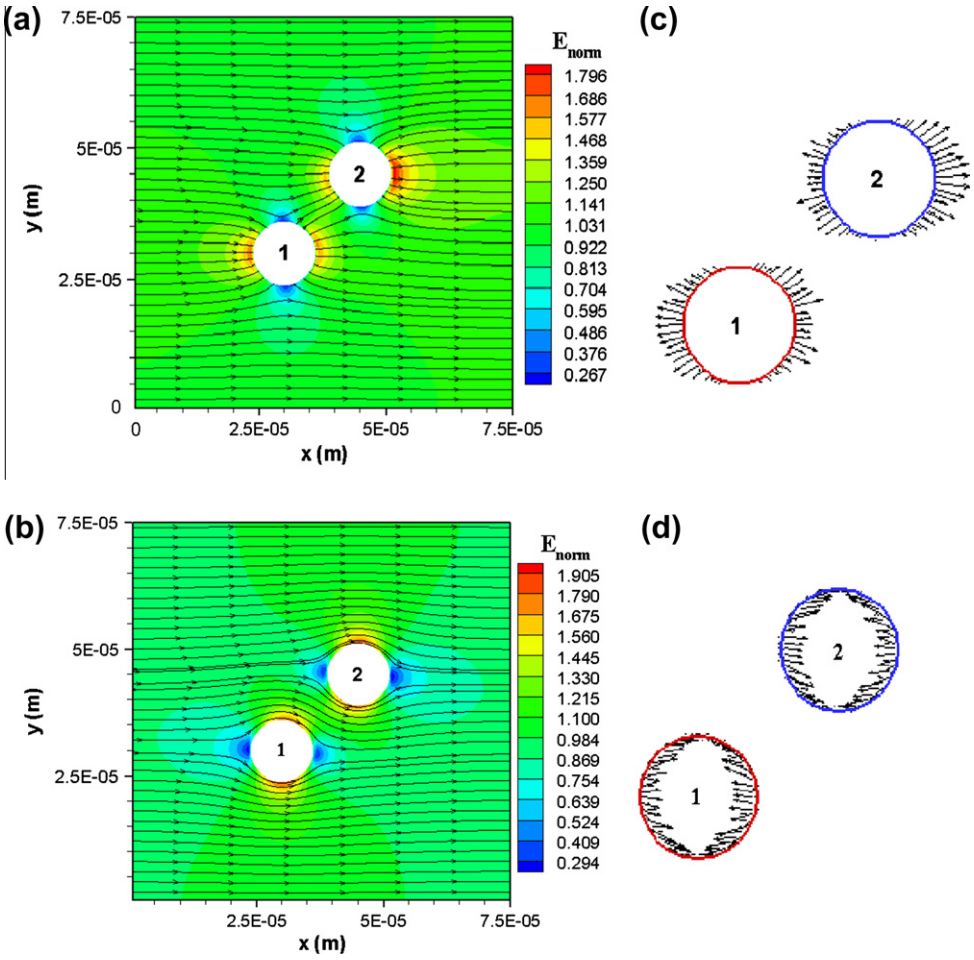

Fig. 2. Two geometrically ($d_1 = d_2 = 12$ μm) and electrically similar particles in a fluid media with an electrical conductivity $\sigma_f = 1.0 \times 10^{-4}$ S/m. Electric field distribution with embedded similar particles for (a) $\sigma_1 = \sigma_2 = 1.0 \times 10^{-3}$ S/m and (b) $\sigma_1 = \sigma_2 = 1.0 \times 10^{-7}$ S/m. The corresponding dielectrophoretic force vector for (c) $\sigma_1 = \sigma_2 = 1.0 \times 10^{-3}$ S/m and (d) $\sigma_1 = \sigma_2 = 1.0 \times 10^{-7}$ S/m. Here the channel dimensions are $a = b = 75$ μm, the initial orientation angle $\theta = 45^0$, and the initial separation distance $d = 22$ μm. The top and bottom surface of the channel is electrically insulating, while electric potentials of 1 V and 0 V are maintained at the left and right boundaries, respectively. The irregularities in the dielectrophoretic force vectors in (c and d) are due to both nonuniform electric field lines and numerical resolution issue. The numerical resolution problem originated from the use of lower order interpolation scheme, and it can be minimized by adopting a higher order interpolation scheme. This kind of resolution issue is also seen in Fig. 4b.

tangent to the particle surface. In this case, the lower electric field regions are found to the left and right hand sides of the particle, and higher electric field regions are created at the top and bottom. The formation of higher and lower electric field regions contributes to dielectrophoretic forces on the particles as shown in Fig. 2c and d for higher and lower conductive particles, respectively. The Eulerian distribution of the dielectrophoretic force was computed using Eq. (21). The dielectrophoretic force is localized near the surface of the particle and is negligible in other regions. This is due to the fact that nonuniformities in electric fields develop near the particle surface because of differences in electrical properties between the particle and the fluid media. It is interesting to note that, in the case of conductive particles, the force vector is tensile in nature, while it is compressive for insulating particles. The nature of force on the particle surface cannot be determined in conventional numerical approaches [21,22], where the net forces are calculated through surface or volumetric integration. The compression or tensile nature of force is very important in biological cell manipulation since it has great impact on cell proliferation and differentiation. For example, in regenerating tissue from mesenchymal into bone, cartilage, or fibrous tissue, compressive stress stimulates chondrogenesis, while high tensile strain stimulates the net production of fibrous tissue [34].

The transient particle–particle interactions of two similar particles ($\sigma_1 = \sigma_2$) are shown in Fig. 3 for an initial separation distance of 22 μm and several initial orientations. For the first two cases, particle conductivity was maintained at 1.0×10^{-7} S/m, while particle conductivity was kept at 1.0×10^{-3} S/m for the last case. At a $\theta = 0^\circ$ orientation (Fig. 3a), the line connecting the centers of the particles is parallel to the electric field and the particles experience

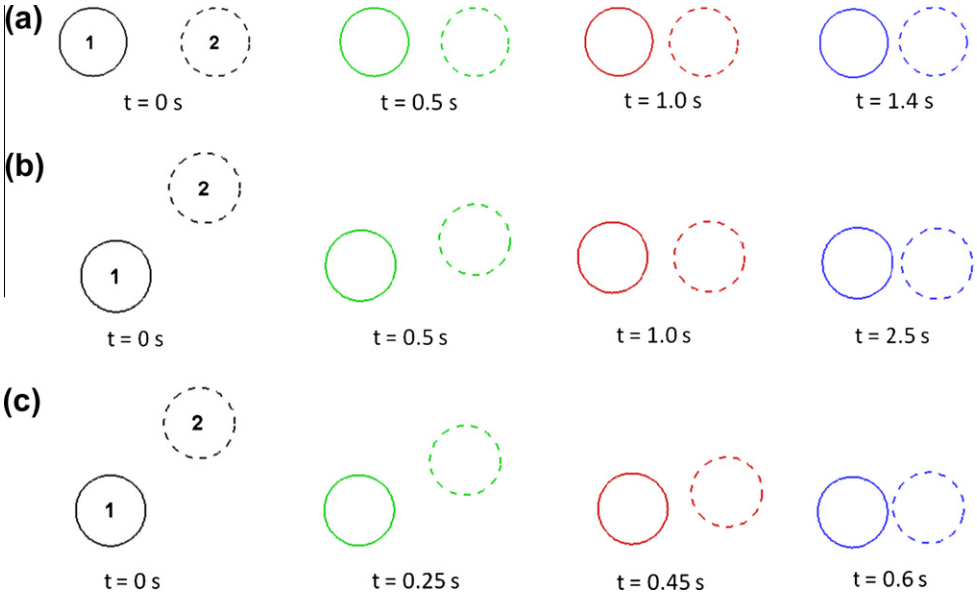

Fig. 3. Predicted locations of particles in the computational domain for similar particle–particle interaction at various initial configurations and particle conductivities: (a) $\theta = 0^0$, $d = 22$ μm, and $\sigma_1 = \sigma_2 = 1.0 \times 10^{-7}$ S/m, (b) $\theta = 45^0$, $d = 22$ μm, and $\sigma_1 = \sigma_2 = 1.0 \times 10^{-7}$ S/m, and (c) $\theta = 45^0$, $d = 22$ μm, and $\sigma_1 = \sigma_2 = 1.0 \times 10^{-3}$ S/m. All other simulation conditions are same as in Fig. 2.

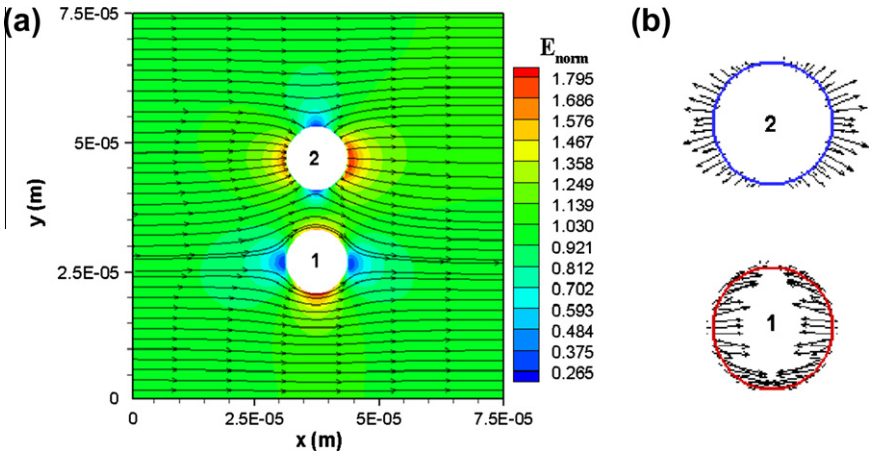

Fig. 4. Two geometrically similar ($d_1 = d_2 = 12$ μm), but electrically dissimilar ($\sigma_1 = 1.0 \times 10^{-7}$ S/m, $\sigma_2 = 1.0 \times 10^{-3}$ S/m) particles in a fluid media with an electrical conductivity of 1.0×10^{-4} S/m. (a) Electric field distribution and (b) the corresponding dielectrophoretic force vector. Here the initial orientation angle $\theta = 90^0$ and the initial separation distance $d = 22$ μm. The top and bottom surface of the channel is electrically insulating, while electric potentials of 1 V and 0 V are maintained at the left and right boundaries, respectively.

an attractive interaction force. Hence, they move toward each other with translational velocity as shown in Fig. 3a. Since the two particles are in close proximity, they distort the surrounding electric field and create a lower electric intensity in the gap between the particles. As the particles are electrically less conductive then the fluid media, the electric field is deflected away from the surface (similar to Fig. 2b) and creates a lower intensity near the surfaces of the particle that faces the electric field orthogonally, in this case the left and right sides of the particle. Distortion of the electric field around the particles creates a negative dielectrophoretic force that moves the particles toward the lower electric field region in the gap. On the other hand, for nonparallel initial orientations with respect to the applied electric field, particles experience both translational and rotational motion with respect to each other (Fig. 3b and c).

Like the case presented in Fig. 3a, the assembly mechanism shown in Fig. 3b was due to negative dielectrophoresis because the particles were less conductive ($\sigma_1 = \sigma_2 = 1.0 \times 10^{-7}$ S/m) than the fluid media. Initially as shown in Fig. 3b, the particles rotate and align themselves parallel to the electric field by a repulsive DEP interaction force and then move toward each other by an attractive DEP interaction force. The simulation results indicate that once the particles align themselves they move faster toward each other but, when they are very close in later time steps, the attractive motion diminishes. The retardation is due to the fact that the degree of nonuniformity in the electric field decreases as the particles approach each other leading to a deceleration [35]. Moreover, as the particles move closer to each other, the opposing hydrodynamic force dominates over the dielectrophoretic interaction force. However, based on the direction and final translational motion of the particles, it is reasonable to conclude that particles velocity approaches zero as they approach each other and form a stable pair. In Fig. 3c, we considered two particles with an initial orientation of 45° and particle conductivity set at $\sigma_1 = \sigma_2 = 1.0 \times 10^{-3}$ S/m. Since the particle conductivity is higher than that of the fluid media, the mechanism of interaction and assembly is positive dielectrophoresis. Thus, particles move toward the higher electric field region, and they assemble themselves faster than particles with less conductivity compared to the media. The accelerating motion of the particles is the result of an increase in positive dielectrophoretic force due to the stronger disruption of the electric field lines in the vicinity of the particle [35]. As in the previous case, the motion of the particles slows down in later time steps as they approach each other. In this study, we also considered a perpendicular orientation ($\theta = 90^0$) of the particles, and the results of this particular case are discussed in Section 4.3.

4.2. Dissimilar particle–particle interaction

In the dissimilar particle–particle interaction case, particle size is kept at $d_1 = d_2 = 12$ μm, while their conductivities are $\sigma_1 = 1.0 \times 10^{-7}$ S/m for the first particle and $\sigma_2 = 1.0 \times 10^{-3}$ S/m for the second. The electric field distributions are shown in Fig. 4a for a perpendicular orientation ($\theta = 90°$) and 22 μm initial separation distance. Simulation results show that the electric field lines are deflected away from the bottom particle surface, while the electric field lines enter orthogonally on the surface of the top particle. This is expected since the bottom particle works as an insulator and the top particle works as a conductor compared to the fluid media. The deflection of the electric field lines around the particle creates a lower electric field zone at the lower end of the top particle and a higher electric field zone at the upper part of the bottom particle as shown in Fig. 4a. Fig. 4b shows the dielectrophoretic particle–particle interaction force vector for this case. The dielectrophoretic force suggests that, in the case of less conductive particles, the force is compressive, but tensile for more conductive particles. These findings are consistent with the observations made in the previous section.

Particle–particle interactions for two dissimilar particles are shown in Fig. 5 for several initial orientations θ. The simulation results indicate that dissimilar particles still attract each other but align themselves perpendicular to the electric field. When two dissimilar particles are in close proximity, the distorted electric field around the particles creates a different electric field intensity in

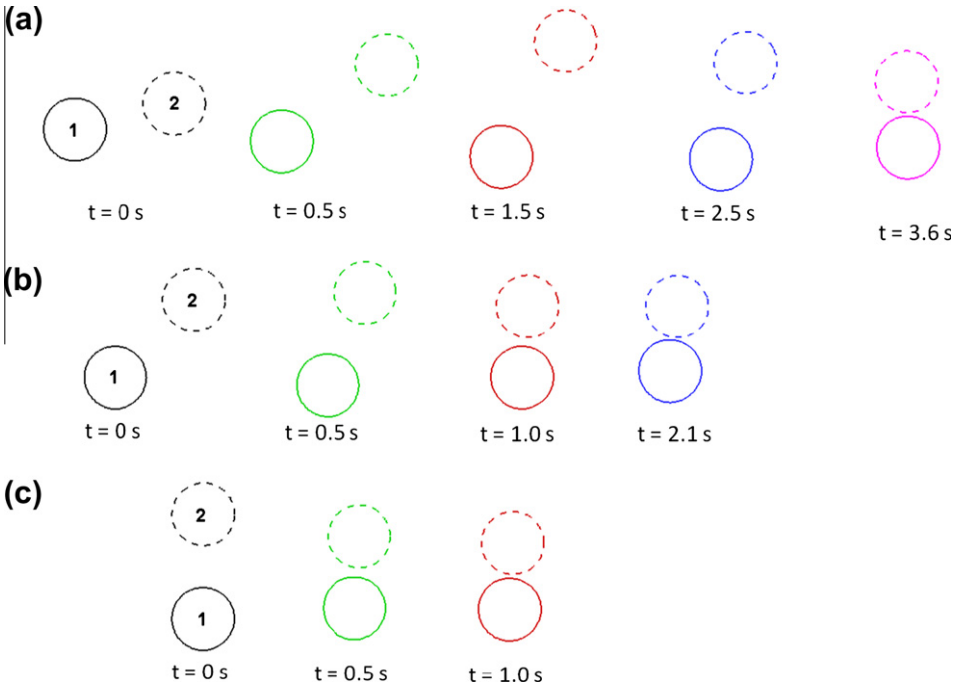

Fig. 5. Predicted locations of particles in the computational domain for dissimilar particle–particle interaction at various initial configurations (a) $\theta = 15^0$, (b) $\theta = 45^0$, and (c) $\theta = 90^0$. For all cases, the initial separations distance $d = 22$ μm. All other simulation conditions are same as in Fig. 4.

the vicinity of each particle. As shown in Fig. 4, a weak electric field is created in the vicinity of the particle whose electrical conductivity is higher than that of the fluid media; a strong electric field is created in the vicinity of the particle that has less conductivity compared to the fluid media. Because of this, the more conductive particle experiences a positive dielectrophoretic interaction force and moves toward the less conductive particle.

On the other hand, the less conductive particle experiences a negative dielectrophoretic interaction force and moves toward the more conductive particle. In the nonperpendicular initial orientation, the dissimilar particles initially align themselves perpendicular to the electric field and then move toward each other to form a perpendicular assembly as shown in Fig. 5a–b. It is interesting to note that in the nonperpendicular initial orientation, one particle rotates in a clockwise and the second rotates in a counter clockwise direction. In the similar particle–particle interaction case, both particles rotate in either a clockwise or a counter clockwise direction depending on the initial orientation.

4.3. Unstable configuration in particle interaction

For similar particles, unstable configurations are found when particles are at a perpendicular orientation ($\theta = 90°$). The electric field lines and the dielectrophoretic movement of particles are shown in Fig. 6a and b, respectively. In this case, particles are less conductive than the fluid ($\sigma_1 = \sigma_2 = 1.0 \times 10^{-7}$ S/m). The appearance of strong and weak electric field regions around the particles is consistent with the electrical conductivities of the particle and media as explained in earlier sections. Numerical results show that instead of chain formation, the particles move away from each other due to the repulsive negative dielectrophoretic interaction force. This happens because particles create higher electric field regions (Fig. 6a) in the gap between particles when they are perfectly aligned perpendicular to the applied electric field. In negative DEP interaction, the particles try to escape from the higher electric field region and hence separate from each other. However, particles become stationary after they reach a certain threshold distance, where the nonuniformity in the electric field due to the presence of neighboring particles is negligible.

In the case of electrically dissimilar particles ($\sigma_1 = 1.0 \times 10^{-7}$ S/m and $\sigma_2 = 1.0 \times 10^{-3}$ S/m), an unstable orientation was found when particles were parallel to the applied electric field. In this configuration, the particles were forced away from each other by a repulsive dielectrophoretic interaction force. The mechanism of this repulsive interaction force can be attributed to both positive and negative dielectrophoresis.

Fig. 6c shows that the gap between the particles has simultaneous lower and higher electric field regions. A higher electric field is found in the vicinity of the electrically higher conductive particle, and a lower electric field is found near the electrically lower

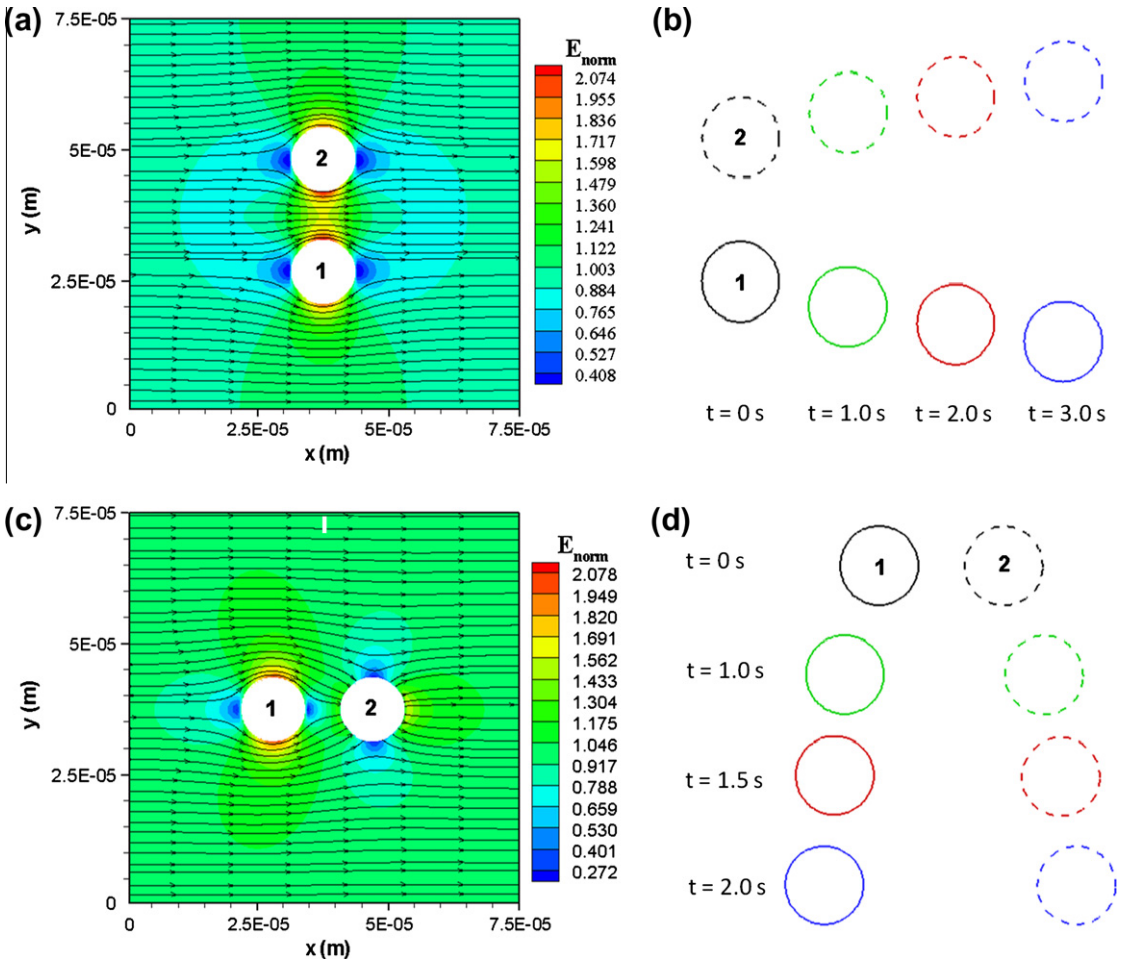

Fig. 6. Simulation results of unstable configurations. (a) Electric field and (b) the corresponding transient locations of particles for two similar type of particles ($\sigma_1 = \sigma_2 = 1.0 \times 10^{-7}$ S/m) with an initial separation distance $d = 22$ μm and at an initial orientation $\theta = 0^0$ (c) Electric field and (d) the corresponding transient locations of particles for two dissimilar type of particles $\sigma_1 = 1.0 \times 10^{-7}$ S/m and $\sigma_2 = 1.0 \times 10^{-3}$ S/m) with an initial separation distance $d = 19$ μm and an initial orientation $\theta = 90^0$ All other simulation conditions are same as in Fig. 2.

conductive particle. Therefore, the more conductive particle experiences positive dielectrophoresis and moves away from its adjacent lower electric field region. On the other hand, the less conductive particle experiences negative dielectrophoresis. It tries to escape from the higher electric field region and translates away until the interaction force becomes negligible. As in the previous case, in this unstable configuration, no chain formation was observed.

4.4. Three particle interaction

Our numerical scheme can be extended for multiple particle interactions. With multiple particles the interactions between particles become more complex, and many parameters are involved. Here, we present simulation results for three particle interaction considering similar and dissimilar particles. First, consider the similar particle case with the computational domain as shown in Fig. 7a. Fig. 7b illustrates the electric field lines for interactions of three similar particles suspended in water. It was assumed that particles were initially orientated in an equilateral triangular fashion, and the conductivity of the particles was assumed to be $\sigma_1 = \sigma_2 = \sigma_3 = 1.0 \times 10^{-7}$ S/m. For the configuration shown in Fig. 7a, the lowest electric field is created in the gap between the two horizontally orientated particles, and localized higher electric field regions were created at the top and bottom of each particle. The transient particle orientation is shown in Fig. 7c. The simulation results show that the particles reorient themselves parallel to the electric field and form a chain as in the two particle case presented earlier. This is due to negative dielectrophoretic particle–particle interaction forces explained earlier for the two particle cases. It is interesting to note that the bottom particle moves upward between the horizontal particles by pushing them toward the sides. Although the lowest electric field region was between the horizontal particles, the horizontal particles could not move toward each other because of the strong electric field region of the bottom particle. The relative distance between particles is also a very important parameter for multiple particle assembly.

To investigate multiple particle interaction of dissimilar particles, a slightly different configuration is considered (Fig. 8a). In this case, a dissimilar particle with conductivity $\sigma_2 = 1.0 \times 10^{-3}$ S/m was placed between similar particles with conductivities $\sigma_1 = \sigma_3 = 1.0 \times 10^{-7}$ S/m. Unlike the previous case, particle–particle distances were different since in a real device the distance between particles is not necessarily the same. The distance between the top and the middle particle was set at 19.75 μm, where the distance between the middle and the bottom particle was 20.5 μm. The electric field distribution for this case is shown in Fig. 8b. The simulation results show that dissimilar particles align themselves perpendicular to the applied electric field by the mechanism for the two particle case explained in Section 4.2. Here, the closest particles align themselves before moving together to align with the third particle. The closer particle has greater affinity due to the disturbance in the local electric field. Based on the results above, this suggests that dielectrophoretic particle–particle interaction generally leads to the chaining of particles and alignment to the electric field regardless of initial particle orientation (except unstable

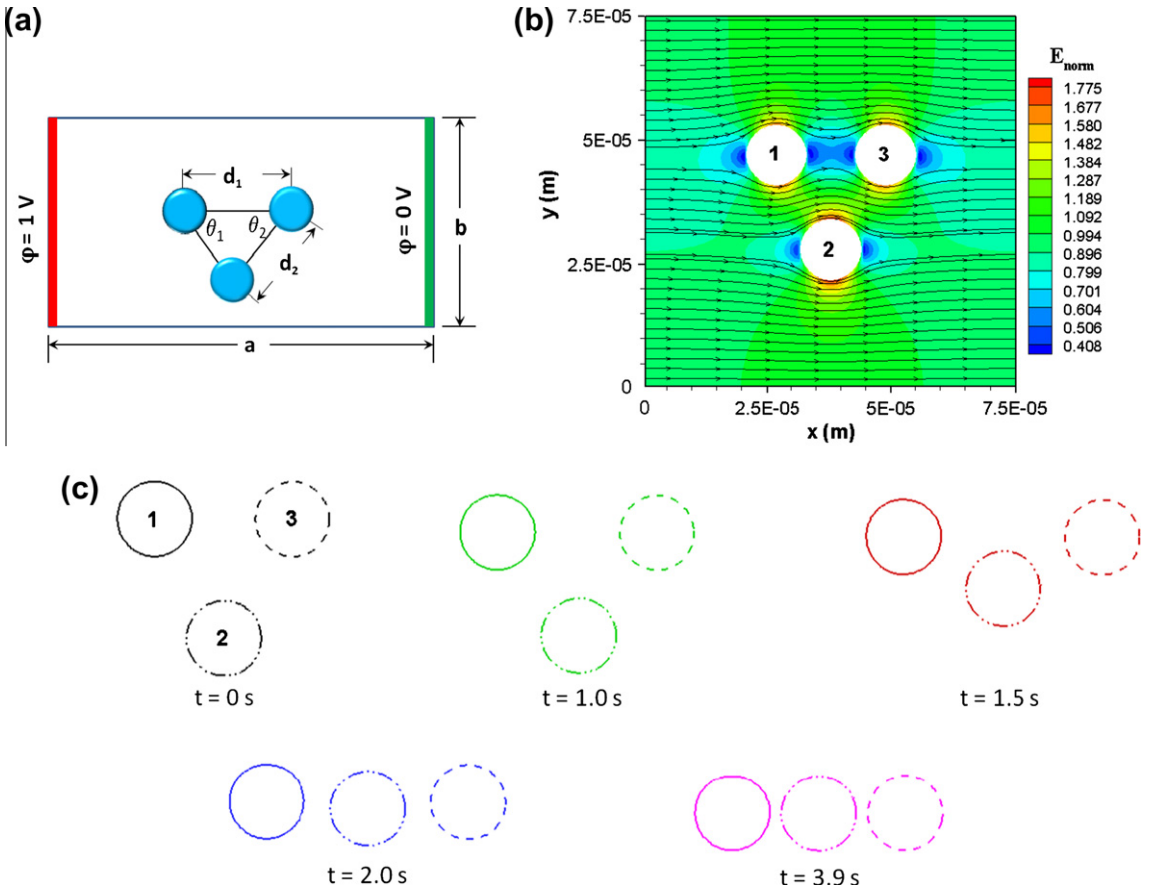

Fig. 7. (a) Computational domain for three similar type particle interactions and assembly in a microfluidic device. The electrodes are placed in left and right boundary while the top and bottom boundaries are insulated. (b) Electric field distributions for three similar type particle ($\sigma_1 = \sigma_2 = \sigma_3 = 1.0 \times 10^{-7}$ S/m) interaction. (c) Transient locations of particles in the computational domain. Here initial orientation angles are $\theta_1 = 60^0$, $\theta_2 = 60^0$, initial separation distances are $d_1 = d_2 = 21$ μm, and channel dimensions are $a = b = 75$ μm. All other simulation conditions are same as in Fig. 2.

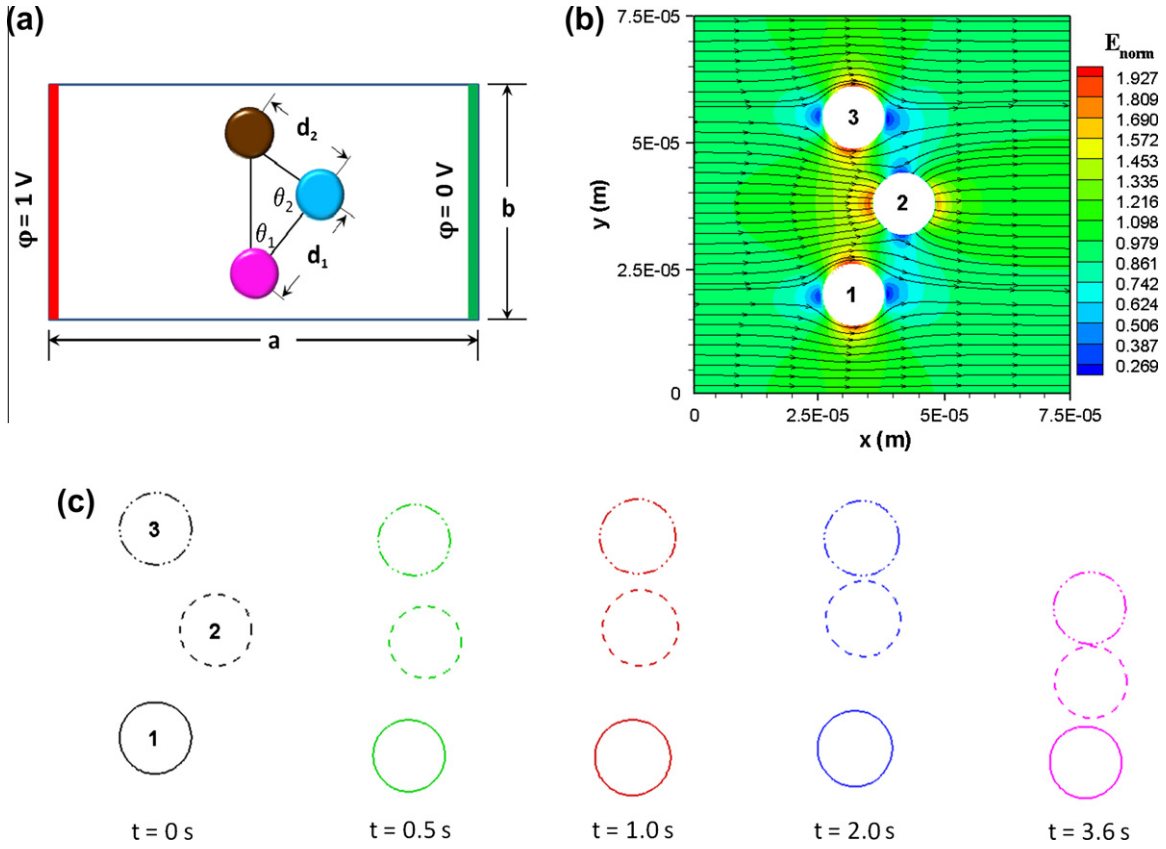

Fig. 8. (a) Computational domain for three particle interactions and assembly in a microfluidic device. The electrodes are placed in left and right boundary while the top and bottom boundaries are insulated. (b) Electric field distributions for three dissimilar type particle ($\sigma_1 = \sigma_3 = 1.0 \times 10^{-7}$ S/m, $\sigma_2 = 1.0 \times 10^{-3}$ S/m) interaction. (c) Transient locations of particles in the computational domain. Here initial orientation angles are $\theta_1 = 30^0$, $\theta_2 = 120^0$, initial separation distances are $d_1 = 20.5$ μm, $d_2 = 19.75$ μm. All other simulation conditions are same as in Fig. 7.

orientations) and the number of particles. Similar experimental observations were also reported in the literature [36].

5. Conclusions

A hybrid immersed interface-immersed boundary method has been employed to investigate the fundamental mechanics of dielectrophoretic particle–particle interaction and multi-particle assembly. Fluid flow has been solved with an immersed boundary method, while the electrostatic problem has been solved with an immersed interface method. The induced electric field force was obtained from Maxwell's stress tensor in Eulerian form by considering the whole domain. This approach mimics the actual physics of electric field induced assembly processes. Although a constant potential difference is applied across the channel, particle–particle interaction forces develop around each particle due to the local nonuniformity of the electric field induced by the presence of particles. We demonstrated particle–particle interaction and particle assembly for two and three similar and dissimilar particles and several initial orientations. This method can be extended to any number of particle assembly and multiple particle–particle interactions. This numerical study provides following conclusions:

1. Localized higher and lower electric field regions around a particle depend on the properties of fluid and particles.
2. Electrically similar particles, regardless of number, initial orientation (except unstable orientation) and polarizability, form chains parallel to the applied electric field. On the other hand, electrically dissimilar particles form chains perpendicular to an applied electric field.
3. The unstable orientations for similar and dissimilar particles are perpendicular and parallel to the applied electric field, respectively.
4. In the assembly process, positive dielectrophoresis provides faster chain formation/assembly than negative dielectrophoresis.
5. In the case of inclined initial orientations, particles rotate and align themselves with respect to the applied electric field first by repulsive DEP interaction force and then translate toward each other by an attractive DEP interaction force.

Acknowledgments

This work was partly supported by the Air Force Office of Scientific Research and partly by the National Science Foundation under Grant No. CTS 1250107.

References

[1] K. Zhu, A.S. Kaprelyants, E.G. Salina, G.H. Markx, Biomicrofluidics 4 (2010).
[2] U. Kim, J. Qian, S.A. Kenrick, P.S. Daugherty, H.T. Soh, Anal. Chem. 80 (2008) 8656.
[3] J. Voldman, M. Toner, M.L. Gray, M.A. Schmidt, J. Electrostatics 57 (2003) 69.
[4] P. Gascoyne, C. Mahidol, M. Ruchirawat, J. Satayavivad, P. Watcharasit, F.F. Becker, Lab Chip 2 (2002) 70.
[5] B.H. Lapizco-Encinas, B.A. Simmons, E.B. Cummings, Y. Fintschenko, Anal. Chem. 76 (2004) 1571.
[6] K.L. Chan, H. Morgan, E. Morgan, I.T. Cameron, M.R. Thomas, Biochimica Et Biophysica Acta – Molecular Basis of Disease 1500 (2000) 313.

[7] S.O. Lumsdon, E.W. Kaler, O.D. Velev, Langmuir 20 (2004) 2108.
[8] M. Yang, X. Zhang, Sens. Actuators, A – Phys. 135 (2007) 73.
[9] O.D. Velev, E.W. Kaler, Langmuir 15 (1999) 3693.
[10] N. Aubry, P. Singh, M. Janjua, S. Nudurupati, Proc. Natl Acad. Sci. U. S. A. 105 (2008) 3711.
[11] O.D. Velev, K.H. Bhatt, Soft Matter 2 (2006) 738.
[12] X. Xiong, A. Busnaina, S. Selvarasah, S. Somu, M. Wei, J. Mead, C.L. Chen, J. Aceros, P. Makaram, M.R. Dokmeci, Appl. Phys. Lett. 91 (2007).
[13] B.M.I. van der Zande, G.J.M. Koper, H.N.W. Lekkerkerker, J. Phys. Chem. B 103 (1999) 5754.
[14] J.Y. Chung, K.H. Lee, J.H. Lee, R.S. Ruoff, Langmuir 20 (2004) 3011.
[15] G.H. Markx, L. Carney, M. Littlefair, A. Sebastian, A.-M. Buckle, Biomed. Microdevices 11 (2009) 143.
[16] S. Gupta, R.G. Alargova, P.K. Kilpatrick, O.D. Velev, Soft Matter 4 (2008) 726.
[17] H. Hwang, J.J. Kim, J.K. Park, J. Phys. Chem. B 112 (2008) 9903.
[18] K.H. Kang, D.Q. Li, Langmuir 22 (2006) 1602.
[19] J. Kadaksham, P. Singh, N. Aubry, J. Fluids Eng. – Trans. ASME 126 (2004) 170.
[20] N. Aubry, P. Singh, Europhys. Lett. 74 (2006) 623.
[21] Y. Ai, S.Z. Qian, J. Colloid Interface Sci. 346 (2010) 448.
[22] D.L. House, H.X. Luo, S.Y. Chang, J. Colloid Interface Sci. 374 (2012) 141.
[23] H.A. Pohl, Dielectrophoresis – The Behavior of Neutral Matter in Nonuniform Electric Fields, Cambridge University Press, Great Britain, 1978.
[24] C.S. Peskin, J. Comput. Phys. (1977) 220.
[25] C.-Y. Hsu, R. Dillon, Bull. Math. Biol. 71 (2009) 1228.
[26] R. Dillon, H.G. Othmer, J. Theor. Biol. 197 (1999) 295.
[27] Z.L. Li, SIAM J. Numer. Anal. 35 (1998) 230.
[28] G.H. Markx, R. Pethig, J. Rousselet, J. Phys. D – Appl. Phys. 30 (1997) 2470.
[29] P. Dutta, A. Beskok, T. Warburton, Numer. Heat Transfer Part A – Appl. 41 (2002) 131.
[30] M. Hossan, R. Dillon, P. Dutta, J. Comput. Phys. (submitted for publication).
[31] O. Schenk, K. Gartner, Electron. Trans. Numer. Anal. 23 (2006) 158.
[32] O. Schenk, A. Wachter, M. Hagemann, Comput. Optimiz. Appl. 36 (2007) 321.
[33] D.M. McQueen, C.S. Peskin, Comput. Graphics-Us 34 (2000) 56.
[34] D.R. Carter, G.S. Beaupre, N.J. Giori, J.A. Helms, Clin. Orthopaedics Related Res. (1998) S41.
[35] C.H. Kua, Y.C. Lam, I. Rodriguez, C. Yang, K. Youcef-Toumi, Anal. Chem. 80 (2008) 5454.
[36] U. Zimmermann, U. Friedrich, H. Mussauer, P. Gessner, K. Hamel, V. Sukhoruhov, IEEE Trans. Plasma Sci. 28 (2000) 72.